

Phonon counting and intensity interferometry of a nanomechanical resonator

Justin D. Cohen^{1*}, Seán M. Meenehan^{1*}, Gregory S. MacCabe¹, Simon Gröblacher^{1,2†}, Amir H. Safavi-Naeini^{1,3}, Francesco Marsili⁴, Matthew D. Shaw⁴ & Oskar Painter¹

In optics, the ability to measure individual quanta of light (photons) enables a great many applications, ranging from dynamic imaging within living organisms¹ to secure quantum communication². Pioneering photon counting experiments, such as the intensity interferometry performed by Hanbury Brown and Twiss³ to measure the angular width of visible stars, have played a critical role in our understanding of the full quantum nature of light⁴. As with matter at the atomic scale, the laws of quantum mechanics also govern the properties of macroscopic mechanical objects, providing fundamental quantum limits to the sensitivity of mechanical sensors and transducers. Current research in cavity optomechanics seeks to use light to explore the quantum properties of mechanical systems ranging in size from kilogram-mass mirrors to nanoscale membranes⁵, as well as to develop technologies for precision sensing⁶ and quantum information processing^{7,8}. Here we use an optical probe and single-photon detection to study the acoustic emission and absorption processes in a silicon nanomechanical resonator, and perform a measurement similar to that used by Hanbury Brown and Twiss to measure correlations in the emitted phonons as the resonator undergoes a parametric instability formally equivalent to that of a laser⁹. Owing to the cavity-enhanced coupling of light with mechanical motion, this effective phonon counting technique has a noise equivalent phonon sensitivity of 0.89 ± 0.05 . With straightforward improvements to this method, a variety of quantum state engineering tasks using mesoscopic mechanical resonators would be enabled¹⁰, including the generation and heralding of single-phonon Fock states¹¹ and the quantum entanglement of remote mechanical elements^{12,13}.

Measurement of the properties of mechanical systems in the quantum regime typically involves heterodyne detection of a coupled optical or electrical field, yielding a continuous signal proportional to the displacement amplitude¹⁴. An alternative method, particularly suited to optical read-out, is to utilize photon counting as a means to probe the quantum dynamics of the coupled optomechanical system^{15,16}. Photon counting can be readily adapted to study intensity correlations in an optical field, and has been used not only in the astronomical studies of thermal light using the technique of Hanbury Brown and Twiss (HBT), but also in early studies of the photon statistics of laser light and single-atom fluorescence^{4,17}. In the field of photon-correlation spectroscopy, such intensity interferometry techniques have found widespread application in the measurement of particle and molecular motion in materials¹⁸. More recently, photon counting of Raman scattering events in diamond has heralded and verified the quantum entanglement of a terahertz phonon shared between two separate bulk diamond crystals¹³. In the case of engineered cavity optomechanical systems, much longer phonon coherence times are attainable, albeit at lower mechanical frequencies (megahertz to gigahertz), which limit the temperature of operation

and the optical power handling capability of such structures. Quantum optical schemes for manipulation of the quantum state of motion in cavity optomechanical systems thus rely on a large per-phonon scattering rate and efficient detection of scattering events. Here we embed a high-Q, gigahertz-frequency mechanical resonator inside an optical nanocavity, greatly enhancing the phonon–photon coupling rate and channelling optical scattering into a preferred optical mode for collection. Single-photon detection of this scattered light then allows for a precise counting of single-phonon emission or absorption events, effectively phonon counting (although this terminology should not be confused with Fock state detection or quantum non-demolition measurement of phonon number). The highly engineered and optimized nature of this optomechanical resonator furthermore yields a sub-phonon-level counting sensitivity of the intracavity mechanical resonator occupancy.

A conceptual schematic of the phonon counting experiment is shown in Fig. 1a. The device consists of a patterned silicon nanobeam which forms an optomechanical crystal (OMC)^{19,20} able to co-localize acoustic (mechanical) and optical resonances at frequencies ω_m and ω_c , respectively. Finite-element-method simulations of the acoustic and optical resonances are shown at the top of Fig. 1a. The Hamiltonian describing the interaction between the acoustic and optical modes is given by $\hat{H}_{\text{int}} = \hbar g_0 \hat{a}^\dagger \hat{a} (\hat{b} + \hat{b}^\dagger)$, where \hat{a} (\hat{b}) is the annihilation operator for the optical (acoustic) mode, and g_0 is the optomechanical coupling rate, physically representing the optical frequency shift due to the zero-point motion of the acoustic resonator. This interaction modulates a laser probe with frequency ω_l to produce sidebands at frequencies $\omega_l \pm \omega_m$, analogous to the anti-Stokes and Stokes sidebands in Raman scattering and corresponding to phonon absorption or emission, respectively. For a system in the resolved sideband limit, where $\omega_m \gg \kappa$ (κ is the linewidth of the optical resonance), the density of states of the optical cavity can be used to resonantly enhance either scattering process for an appropriately detuned pump. In particular, applying a large coherent pump red (blue) detuned from the optical cavity resonance by $\Delta = \omega_c - \omega_l = \omega_m$ ($\Delta = -\omega_m$) results in an effective interaction Hamiltonian of the form $\hat{H}_{\text{int}} = \hbar G (\hat{a}^\dagger \hat{b} + \hat{a} \hat{b}^\dagger)$ ($\hat{H}_{\text{int}} = \hbar G (\hat{a} \hat{b} + \hat{a}^\dagger \hat{b}^\dagger)$), where $G = g_0 \sqrt{n_c}$ is the parametrically enhanced optomechanical coupling rate (n_c is the intracavity photon number at frequency ω_l due to the pump laser). In this case, the output field annihilation operator \hat{a}_{out} can be shown to consist of a coherent component at frequency ω_l as well as a component at frequency ω_c which is proportional to \hat{b} (\hat{b}^\dagger) (ref. 21). Sending the cavity output through a series of narrowband optical filters centred on the cavity resonance, as shown in Fig. 1a, suppresses the pump so that photon counting events will correspond directly to counting phonon absorption (emission) events²². Subsequently directing the filter output to an HBT set-up in order to measure the second-order photon correlation function $g^{(2)}(\tau)$ (ref. 3) will then result in a direct measurement

¹Institute for Quantum Information and Matter and Thomas J. Watson Senior Laboratory of Applied Physics, California Institute of Technology, Pasadena, California 91125, USA. ²Vienna Center for Quantum Science and Technology (VCQ), Faculty of Physics, University of Vienna, A-1090 Wien, Austria. ³Edward L. Ginzton Laboratory, Stanford University, Stanford, California 94305, USA. ⁴Jet Propulsion Laboratory, California Institute of Technology, Pasadena, California 91109, USA. [†]Present address: Kavli Institute of Nanoscience, Delft University of Technology, Lorentzweg 1, 2628 CJ Delft, The Netherlands.

*These authors contributed equally to this work.

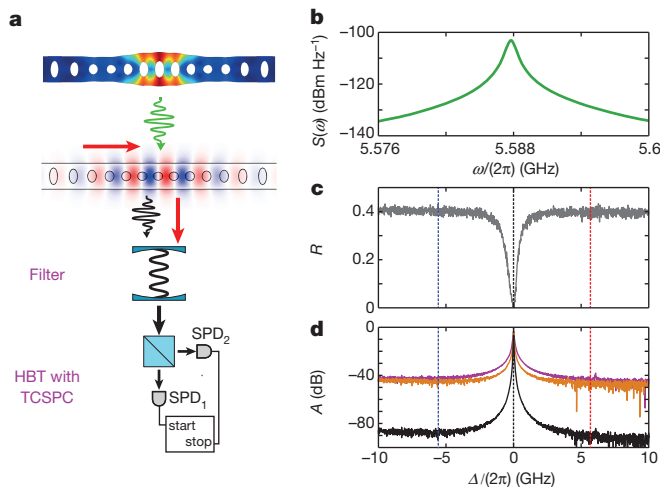


Figure 1 | Phonon counting and device characterization. **a**, Schematic of the phonon counting measurement. The finite element method simulations depict the displacement field of the acoustic resonance (top, blue bar) and the electric field of the optical resonance (next down, bar with no colour filling) of the nanobeam structure. Pump light at optical detuning $\Delta = \pm\omega_m$ is indicated by the red arrows, while the optomechanically scattered sideband light is represented by black arrows. The optical cavity output is filtered to reject the pump, and then detected in a Hanbury Brown and Twiss (HBT) set-up using two superconducting single photon detectors (SPD_{1,2}). The detector outputs are used as start/stop pulses in a time-correlated single photon counting module (TCSPC), yielding the second-order phonon correlation function. **b**, Measured power spectral density $S(\omega)$ of the acoustic resonance. **c**, Normalized optical cavity reflection spectrum, R . Pump detunings of $\Delta = \pm\omega_m/(2\pi) = \pm 5.6$ GHz are indicated by the red and blue dashed lines, respectively. **d**, Transmission spectrum of the first (purple) and second (orange) optical filter, with total filter transmission plotted in black. A is the pump attenuation factor.

of the normally (anti-normally) ordered second-order phonon correlation function. Although this work deals with measurements of a particular cavity optomechanical system, the nanobeam OMC, numerous other geometries possess the requisite optomechanical coupling strength and high mechanical frequency necessary to implement this phonon counting scheme⁵.

As described in ref. 20, the nanobeam is patterned in such a way as to support a ‘breathing’ acoustic resonance at $\omega_m/2\pi = 5.6$ GHz as well as a fundamental optical resonance at a free-space wavelength near 1,550 nm, with a theoretical vacuum coupling rate of $g_0/2\pi = 860$ kHz. All measurements presented here are performed at room temperature and pressure. The thermal Brownian motion of the acoustic resonance manifests as a Lorentzian response centred around ω_m in the noise power spectral density (NPSD), $S(\omega)$, of the cavity reflection photocurrent, as shown in Fig. 1b. The linewidth of this Lorentzian is $\gamma = \gamma_i + \gamma_{\text{OM}}$, where γ_i is the intrinsic acoustic energy damping rate and $\gamma_{\text{OM}} = \pm 4G^2/\kappa$ is the optomechanically induced damping rate due to dynamical back action when pumping on the red or blue sideband, respectively²¹. By measuring this linewidth as a function of n_c for both red and blue detuning, we extract $\gamma_i/2\pi = 3$ MHz and $g_0/2\pi = 645$ kHz. The optical cavity reflection spectrum shown in Fig. 1c reveals a total optical energy decay rate of $\kappa/2\pi = 817$ MHz and a decay rate into the detection channel of $\kappa_c/2\pi = 425$ MHz.

To determine the feasibility of the phonon counting scheme for measurements of the OMC in the quantum regime, one must determine the signal-to-noise ratio (SNR). While the signal level depends on the above-measured optomechanical cavity parameters as well as the overall efficiency of photon detection, any detection events that do not correspond to Raman-scattered sideband photons will contribute as noise. These noise counts originate in dark counts of the single-photon detectors (SPDs) and photodetection of light at frequencies other than ω_c , most notably in the unscattered portion of the laser pump. Two

cascaded tunable, commercially available Fabry–Perot filters (Micron Optics, FFP-TF2), with bandwidths of 50 MHz and free spectral ranges of 20 GHz, are used to attenuate the laser pump by a factor $A > 80$ dB relative to the peak transmission at ω_c (see Fig. 1d). The transmission of the filters is then detected in the HBT apparatus by WSi-based superconducting nanowire SPDs²³ operating at a system detection efficiency of $\eta_{\text{SPD}} \approx 70\%$ and a dark count rate of $\Gamma_{\text{dark}} = 4$ Hz.

A useful parameterization of these quantities is the amount of noise (in units of mechanical occupation quanta) as a proportion of the signal generated by a single phonon in the OMC. Alternatively, this noise-equivalent phonon number n_{NEP} can be interpreted as the mechanical occupation which would produce an SNR of 1. We obtain n_{NEP} then by dividing the noise count rates by the per-phonon sideband photon count rate $\Gamma_{\text{SB},0} = \eta|\gamma_{\text{OM}}|$, where η is the total efficiency of the set-up, including the system efficiency of the SPDs as well as optical insertion loss along the path from cavity to detector. For a coherent pump, this yields:

$$n_{\text{NEP}} = \frac{\kappa^2 \Gamma_{\text{dark}}}{4\eta\kappa_c g_0^2 n_c} + A \left(\frac{\kappa\omega_m}{2\kappa_c g_0} \right)^2 \quad (1)$$

The above equation makes clear the benefits of large cavity-enhanced optomechanical coupling g_0 , both in terms of the low power sensitivity limited by detector dark counts and the high power sensitivity limited by pump bleed-through. Further details about the detection set-up, optical and mechanical spectroscopy, and derivation of n_{NEP} can be found in the Supplementary Information.

In Fig. 2a we show the measured sensitivity of the phonon counting set-up for $\Delta = \omega_m$ (filled grey circles), as well as the expected theoretical curve (dashed line) given by equation (1). The noise count rate is measured with the pump beam detuned far off-resonance from the optical cavity, $\Delta \gg \omega_m$, which eliminates the signal due to motional sideband photons but does not change the reflected pump signal or SPD dark counts. To determine $\Gamma_{\text{SB},0}$, the sideband count rate is measured at low n_c where back action is negligible and the mechanical

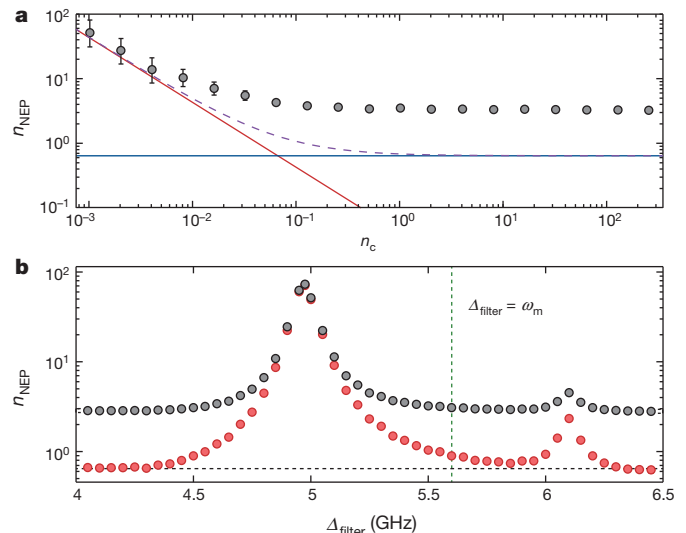


Figure 2 | Phonon counting sensitivity. **a**, Noise equivalent phonon number n_{NEP} versus intracavity photon number n_c calculated using the measured signal and noise count rates for our current set-up (filled grey circles). Solid lines indicate the theoretically expected contributions due to dark counts (red) and pump bleed-through (blue), based on the measured system efficiency and pump suppression, with the sum of the two contributions displayed as a purple dashed line. Error bars show one s.d. determined from the measured count rates, assuming Poissonian counting statistics. **b**, n_{NEP} versus filter–pump detuning Δ_{filter} for $n_c \approx 65$, with (red) and without (grey) an additional C-band band-pass filter inserted. The vertical green line indicates the detuning corresponding to the data from **a**, and the horizontal black line indicates the expected limiting sensitivity.

mode occupancy $\langle n \rangle$ is equal to the room temperature thermal bath occupancy of $n_b \approx 1,100$. Since $\Gamma_{SB,0}$ scales linearly with n_c , we can determine $\Gamma_{SB,0}$ for all n_c from this single measurement without relying on calibration of the optomechanical back action. We can then compute n_{NEP} by dividing this noise count rate by $\Gamma_{SB,0}$ at each value of n_c . The measured sensitivity follows the expected curve at low power due to detector dark counts (solid red curve), but at high n_c saturates to a value several times larger than expected for the filter suppression of the pump (solid blue curve). In order to better understand this excess noise, Fig. 2b shows measurements of the n_{NEP} as a function of filter-pump detuning, Δ_{filter} at a high power where the pump transmission dominates the noise ($n_c \approx 65$). A strong dependence on Δ_{filter} is observed, with a peak in the noise at 5 GHz and a secondary peak at 6.1 GHz, consistent with the phase noise of our pump laser²¹. With the addition of a C-band bandpass filter before the SPD to remove broadband spontaneous emission from the pump laser, and at frequencies far from the laser phase-noise peaks, the measured n_{NEP} agrees well with the theoretical predictions based on the filter pump suppression (horizontal dashed curve). At the relevant detuning of $\Delta_{\text{filter}} = \omega_m$ (vertical dashed curve), we measure a limiting sensitivity of $n_{NEP} = 0.89 \pm 0.05$. While this sensitivity is directly measured at $n_c \approx 65$, n_{NEP} is observed in Fig. 2a to be pump-limited for $n_c \gtrsim 1$, implying that our current set-up achieves $n_{NEP} < 1$ for n_c of order unity.

In what follows, we focus on measurements made with a blue-detuned pump ($\Delta = -\omega_m$), in which the optomechanical back action results in instability and self-oscillation of the acoustic resonator^{9,21}. The Stokes sideband count rate detected on a single SPD, shown versus n_c in Fig. 3a, displays a pronounced threshold, with an exponential increase in output power beginning at $n_c \approx 1,200$, where $C \equiv |\gamma_{OM}|/\gamma_1 \approx 0.8$, in agreement with the expected onset of instability around $C = 1$ ($\gamma = 0$). This sharp oscillation threshold can also be observed from the measured noise power spectral density (NPSD; Fig. 3b), in which the amplitude of the mechanical spectrum is seen to rapidly

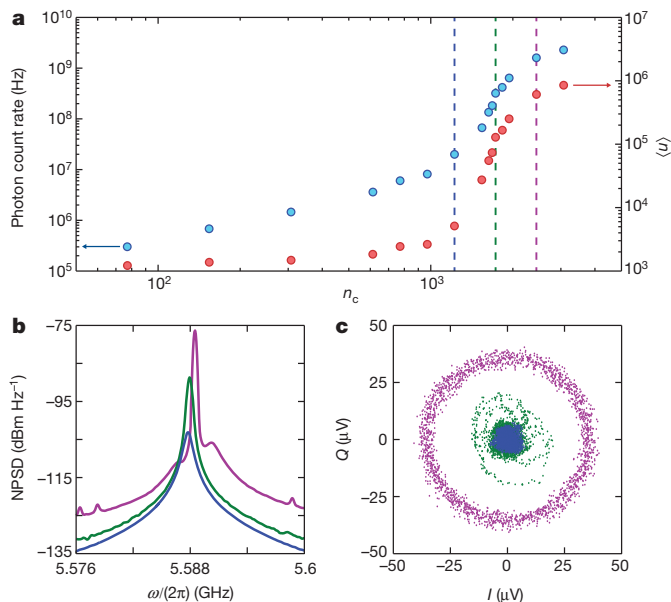


Figure 3 | Phonon lasing. **a**, Phonon count rate (blue: left-hand vertical axis) and inferred phonon occupancy $\langle n \rangle$ (red: right-hand vertical axis) as a function of intracavity photon number n_c for $\Delta = -\omega_m$. Dashed lines indicate points below (blue), at (green) and above (magenta) threshold. **b**, Noise power spectral densities (NPSD) corresponding to the dashed lines in **a**. The small satellite peaks in the thermal emission background of the above-threshold spectrum correspond to beating of the phonon laser line with low-frequency modes of the nanobeam structure. **c**, Phase plots of the in-phase (I) and in-quadrature (Q) amplitudes of the optical heterodyne signal for each of the dashed lines in **a**, acquired in a 36 MHz span around 5.588 GHz over a 60 s time interval.

increase with a simultaneous reduction in linewidth, and in plots of the in-phase and in-quadrature components of the photocurrent fluctuations, which show a transition from thermal noise to a large-amplitude sinusoidal oscillation. Also shown in Fig. 3a is the inferred phonon occupancy $\langle n \rangle$. Below threshold, the photon count rate is related to $\langle n \rangle$ via the simple linear relation $\Gamma_{\text{tot}} = \eta|\gamma_{OM}|(\langle n \rangle + 1)$. At and above threshold, as detailed in the Supplementary Information, self-consistent determination of the oscillation amplitude indicates that even at our highest pump power the mechanical amplitude remains small enough that this linear approximation remains valid.

The statistical properties of the resonator near the self-oscillation threshold can also be characterized by measuring photon correlations using an HBT set-up as shown in Fig. 1. As noted earlier, blue-detuned pumping produces anti-normally ordered phonon correlations. In this case $g^{(2)}(\tau)$ refers to the anti-normally ordered second-order phonon correlation function, defined by $g^{(2)}(\tau) = \langle \hat{b}(0)\hat{b}(\tau)\hat{b}^\dagger(\tau)\hat{b}^\dagger(0) \rangle / \langle \hat{b}(0)\hat{b}^\dagger(0) \rangle^2$. For measurements made with a red-detuned pump, as shown in Fig. 4b, $g^{(2)}(\tau)$ refers to the normally ordered phonon correlation function, $g^{(2)}(\tau) = \langle \hat{b}^\dagger(0)\hat{b}^\dagger(\tau)\hat{b}(\tau)\hat{b}(0) \rangle / \langle \hat{b}^\dagger(0)\hat{b}(0) \rangle^2$. In the case of the classical states measured here, there is no observable difference between

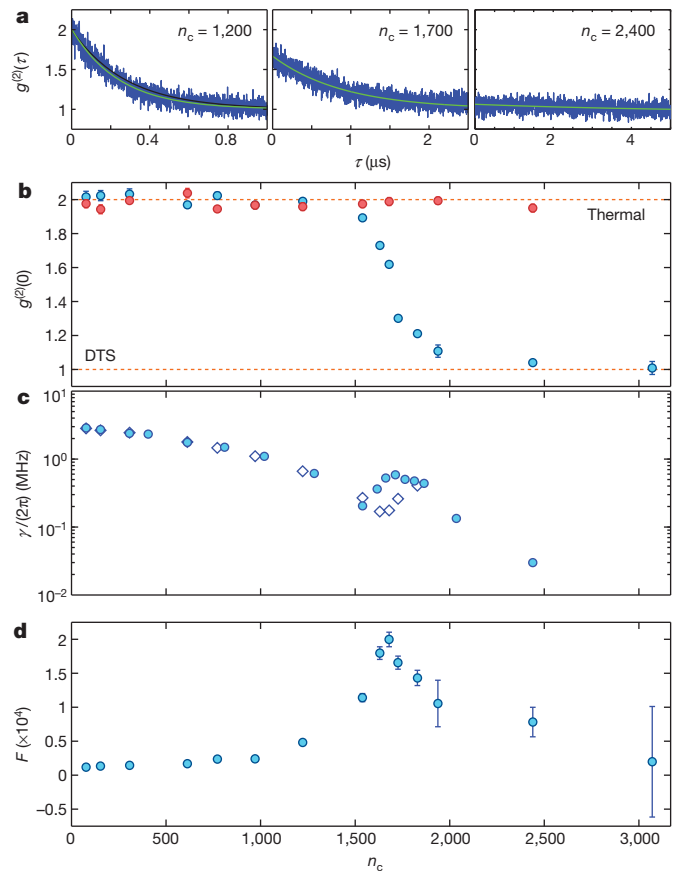


Figure 4 | Phonon intensity correlations. **a**, Normalized anti-normally ordered second-order intensity correlation function $g^{(2)}(\tau)$ for $\Delta = -\omega_m$, shown below, at and above threshold (left, middle and right, respectively). Green lines show a simple exponential fit, while black lines indicate the expected theoretical curve using decay rates measured from fitting the NPSD linewidth. **b**, Phonon correlation at zero time delay versus n_c for $\Delta = -\omega_m$ (blue) and $\Delta = \omega_m$ (red). The top and bottom dashed lines indicate the expected values for purely thermal or displaced thermal states (DTS), respectively. Error bars show one s.d. determined from the fit value of $g^{(2)}(0)$. **c**, Mechanical decay rate versus n_c for $\Delta = -\omega_m$, determined from the measured linewidth of the NPSD (circles) and from the exponential fit to $g^{(2)}(\tau)$ (diamonds). **d**, Fano factor versus n_c . Error bars show one s.d. determined from the measured count rates, assuming Poissonian counting statistics, and the fit value of $g^{(2)}(0)$.

the normally and anti-normally ordered correlation functions. As the oscillation threshold is crossed, the state of the acoustic resonator will transition from a thermal state into a displaced thermal state (DTS), and the normalized phonon intensity correlation function near $\tau = 0$ should show a transition from bunching ($g^{(2)}(0) > 1$) to Poissonian statistics ($g^{(2)}(\tau) = 1$ for all τ). Plots of $g^{(2)}(\tau)$ below, at, and above threshold are shown in Fig. 4a. Below threshold, bunching is clearly visible, with $g^{(2)}(0) = 2$ as expected for a purely thermal state. In Fig. 4b $g^{(2)}(0)$ is plotted versus n_c for both blue- and red-detuned pump light. For a blue-detuned pump, a smooth decrease from $g^{(2)}(0) = 2$ to $g^{(2)}(0) = 1$ is observed in the threshold region, while for a red-detuned pump, the oscillator is observed to remain in a thermal state through threshold and beyond. The decay rate of the acoustic resonator, measured from both the linewidth of the NPSD and from an exponential fit to $g^{(2)}(\tau)$ below threshold, is plotted in Fig. 4c. The decay rate as measured from the NPSD, which includes both phase and amplitude fluctuations, is seen to increase around threshold before continuing to decrease. This behaviour is commonly observed in semiconductor lasers where a coupling exists between the gain and the cavity refractive index, and a similar effect arises in optomechanical oscillators due to the optical spring effect²⁴. The decay rate measured from $g^{(2)}(\tau)$, on the other hand, which measures intensity fluctuations, begins to deviate from the measured linewidth in the vicinity of threshold. Thermal phonon emission dictates a strict correspondence between the second-order and first-order coherence functions⁴; however, above threshold where the phonon statistics are no longer purely thermal, such a deviation is possible, and in fact predicted for self-sustaining oscillators²⁵. The Fano factor, defined as $F = (\Delta n)^2 / \langle n \rangle = 1 + \langle n \rangle (g^{(2)}(0) - 1)$, provides additional statistical information about the fluctuations of the oscillator, and is useful for defining a precise oscillator threshold²⁶ as well as distinguishing between states that may have similar or identical values of $g^{(2)}(0)$ (for example, a coherent state versus a DTS)²⁴. The Fano factor of our mechanical oscillator, computed from the measured $g^{(2)}(0)$ and the inferred values of $\langle n \rangle$, is displayed in Fig. 4d and shows the expected increase and peak in fluctuations at threshold. Above threshold, the Fano factor drops again due to saturation in the optomechanical gain, approaching a measured value consistent with that expected for a DTS ($F \approx 2n_b + 1$).

Although we have emphasized the analogy between the optomechanical oscillator studied here and a laser, there are unique differences which arise owing to the intrinsically nonlinear nature of the radiation pressure interaction in an optomechanical cavity. Recent theoretical studies^{15,24,27} indicate that a laser-driven optomechanical oscillator will enter a non-classical mechanical state with anti-bunched phonon statistics ($F < 1$), and under slightly more restrictive conditions, strongly negative Wigner density. Surprisingly, this is predicted to be observable even for classical parameters, that is, outside the single-photon strong-coupling regime ($g_0/\kappa < 1$), and in the presence of thermal noise. Beyond phonon correlation spectroscopy of optomechanical oscillators, it is envisioned that sensitive photon counting of the filtered motional sidebands may be used in the preparation and heralding of non-Gaussian quantum states of a mechanical resonator¹⁰. For the OMC cavities of this work, with their large optomechanical coupling rate and near millisecond-long thermal decoherence time at temperatures less than 1 K (ref. 28), the phonon addition and subtraction processes of ref. 10 should be realizable with high fidelity and at rates approaching a megahertz. Whether for studies of the quantum behaviour of mesoscopic mechanical objects or in the context of proposed quantum information processing architectures using phonons and photons⁸, such photon counting methods are an attractive way of introducing a quantum nonlinearity into the cavity optomechanical system.

Received 4 October 2014; accepted 10 February 2015.

1. Hoover, E. E. & Squier, J. A. Advances in multiphoton microscopy technology. *Nature Photon.* **7**, 93–101 (2013).

2. Hadfield, R. H. Single-photon detectors for optical quantum information applications. *Nature Photon.* **3**, 696–705 (2009).
3. Hanbury Brown, R. & Twiss, R. Q. A test of a new type of stellar interferometer on Sirius. *Nature* **178**, 1046–1048 (1956).
4. Glauber, R. J. The quantum theory of optical coherence. *Phys. Rev.* **130**, 2529–2539 (1963).
5. Aspelmeyer, M., Kippenberg, T. J. & Marquardt, F. Cavity optomechanics. *Rev. Mod. Phys.* **86**, 1391–1452 (2014).
6. Suh, J. *et al.* Mechanically detecting and avoiding the quantum fluctuations of a microwave field. *Science* **344**, 1262–1265 (2014).
7. Stannigel, K., Rabl, P., Sørensen, A. S., Lukin, M. D. & Zoller, P. Optomechanical transducers for quantum-information processing. *Phys. Rev. A* **84**, 042341 (2011).
8. Stannigel, K. *et al.* Optomechanical quantum information processing with photons and phonons. *Phys. Rev. Lett.* **109**, 013603 (2012).
9. Grudinin, I. S., Lee, H., Painter, O. & Vahala, K. J. Phonon laser action in a tunable two-level system. *Phys. Rev. Lett.* **104**, 083901 (2010).
10. Vanner, M. R., Aspelmeyer, M. & Kim, M. S. Quantum state orthogonalization and a toolset for quantum optomechanical phonon control. *Phys. Rev. Lett.* **110**, 010504 (2013).
11. Galland, C., Sangouard, N., Piro, N., Gisin, N. & Kippenberg, T. J. Heralded single-phonon preparation, storage, and readout in cavity optomechanics. *Phys. Rev. Lett.* **112**, 143602 (2014).
12. Børkje, K., Nunnenkamp, A. & Girvin, S. M. Proposal for entangling remote micromechanical oscillators via optical measurements. *Phys. Rev. Lett.* **107**, 123601 (2011).
13. Lee, K. C. *et al.* Entangling macroscopic diamonds at room temperature. *Science* **334**, 1253–1256 (2011).
14. Clerk, A. A., Devoret, M. H., Girvin, S. M., Marquardt, F. & Schoelkopf, R. J. Introduction to quantum noise, measurement, and amplification. *Rev. Mod. Phys.* **82**, 1155–1208 (2010).
15. Qian, J., Clerk, A. A., Hammerer, K. & Marquardt, F. Quantum signatures of the optomechanical instability. *Phys. Rev. Lett.* **109**, 253601 (2012).
16. Kronwald, A., Ludwig, M. & Marquardt, F. Full photon statistics of a light beam transmitted through an optomechanical system. *Phys. Rev. A* **87**, 013847 (2013).
17. Kimble, H. J., Dagenais, M. & Mandel, L. Photon antibunching in resonance fluorescence. *Phys. Rev. Lett.* **39**, 691–695 (1977).
18. Pike, R. 50th anniversary of the laser. *J. Eur. Opt. Soc. Rapid Publ.* **5**, 10047s (2010).
19. Chan, J. *et al.* Laser cooling of a nanomechanical oscillator into its quantum ground state. *Nature* **478**, 89–92 (2011).
20. Chan, J., Safavi-Naeini, A. H., Hill, J. T., Meenehan, S. & Painter, O. Optimized optomechanical crystal cavity with acoustic radiation shield. *Appl. Phys. Lett.* **101**, 081115 (2012).
21. Safavi-Naeini, A. H. *et al.* Laser noise in cavity-optomechanical cooling and thermometry. *New J. Phys.* **15**, 035007 (2013).
22. Fetter, A. L. Intensity correlations in Raman scattering. *Phys. Rev.* **139**, A1616–A1623 (1965).
23. Marsili, F. *et al.* Detecting single infrared photons with 93% system efficiency. *Nature Photon.* **7**, 210–214 (2013).
24. Rodrigues, D. A. & Armour, A. D. Amplitude noise suppression in cavity-driven oscillations of a mechanical resonator. *Phys. Rev. Lett.* **104**, 053601 (2010).
25. Lax, M. Classical noise. V. Noise in self-sustained oscillators. *Phys. Rev.* **160**, 290–307 (1967).
26. Rice, P. R. & Carmichael, H. J. Photon statistics of a cavity-QED laser: a comment on the laser-phase-transition analogy. *Phys. Rev. A* **50**, 4318–4329 (1994).
27. Lörch, N., Qian, J., Clerk, A., Marquardt, F. & Hammerer, K. Laser theory for optomechanics: limit cycles in the quantum regime. *Phys. Rev. X* **4**, 011015 (2014).
28. Meenehan, S. M. *et al.* Silicon optomechanical crystal resonator at millikelvin temperatures. *Phys. Rev. A* **90**, 011803 (2014).

Supplementary Information is available in the online version of the paper.

Acknowledgements We thank F. Marquardt and A. G. Krause for discussions, and V. B. Verma, R. P. Miriam and S. W. Nam for their help with the single-photon detectors used in this work. This work was supported by the DARPA ORCHID and MESO programmes, the Institute for Quantum Information and Matter, an NSF Physics Frontiers Center with the support of the Gordon and Betty Moore Foundation, and the Kavli Nanoscience Institute at Caltech. Part of the research was carried out at the Jet Propulsion Laboratory, California Institute of Technology, under a contract with NASA. A.H.S.-N. acknowledges support from NSERC. S.G. was supported by a Marie Curie International Out-going Fellowship within the 7th European Community Framework Programme.

Author Contributions O.P., S.M.M., J.D.C., S.G. and A.H.S.-N. planned the experiment. J.D.C., S.G., G.S.M., S.M.M. and A.H.S.-N. performed the device design and fabrication. F.M. and M.D.S. provided the single-photon detectors along with technical support for their installation and running. J.D.C., S.M.M., G.S.M. and O.P. performed the measurements, analysed the data and wrote the manuscript.

Author Information Reprints and permissions information is available at www.nature.com/reprints. The authors declare no competing financial interests. Readers are welcome to comment on the online version of the paper. Correspondence and requests for materials should be addressed to O.P. (opainter@caltech.edu).